Lidar sounding of water, soil, and plants

F.V. Bunkin and A.F. Bunkin

Institute of General Physics,
Russian Academy of Sciences, Moscow
Scientific Center for Wave Research, Moscow

Received December 20, 1999

The paper presents the results of laboratory and field experiments which demonstrate the capabilities of the versatile lidar developed. The lidar is designed for monitoring the ecological state of water, soil, and vegetation. In particular, parallel measurements of the fluorescence spectra of soil, plants, and sea water reveal close agreement of their main spectral features. It was found that the spectra of the return signals from samples of sea water varied with time. This variability is indicative of the need for *in situ* fast analysis of water media.

Introduction

The rapid increase of environmental pollution has aroused a growing interest in the development of techniques and instrumentation for rapid measurements of pollutant content of the atmosphere, water bodies, soil, and vegetation. Lidar sounding is an effective approach to the solution of such problems,[1–3] since it allows real-time acquisition of sufficiently complete information about the medium under study, including the case of airborne measurements.[2–4] Such measurements are often used for calibration (ground-truthing) of satellite images of the Earth's surface.[5,6] However, most currently available lidar systems have large size and insufficient versatility. We have designed and built a compact fluorescent lidar to be used for sounding of water bodies, soil, and plants from on board helicopters, motor vehicles, and ships. This paper presents results of field and laboratory experiments which illustrate the capabilities of such sounding.

Experiment

The optical layout of the lidar is shown in Fig. 1. As the radiation source, the lidar employed a specialized vibration-resistant Nd:YAG laser with the following parameters:

pulse duration	8 ns
pulse repetition frequency	up to 25 Hz
energy per pulse for the first harmonic (1064 nm)	600 mJ
energy per pulse for the second harmonic (532 nm)	280 mJ
energy per pulse for the third harmonic (354 nm)	100 mJ

The metal mirror *7* directs the sounding beam toward the investigated object (water body, soil, plant canopy). In addition, this mirror reflects the return signal being recorded onto the receiving mirror of the telescope *6* (relative aperture 1/3, diameter 200 mm). The return signal is then focused through the specialized input device *4* onto the entrance slit of the autocollimation polychromator *5*. The polychromator employs diffraction gratings of 300 and 1200 lines/mm, and the dispersion of the polychromator (300 lines/mm grid) is 42 nm/mm in the first diffraction order and 2 nm/mm in the ninth diffraction order.

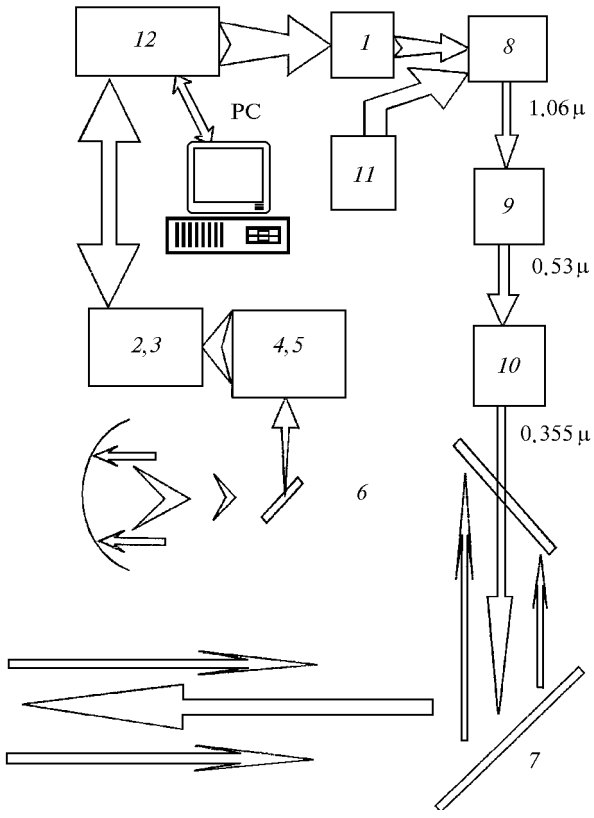

Fig. 1. Optical layout of the lidar.

0235-6880/00/01 54-07 $02.00

Spectra of the return signals at the polychromator output are recorded by a cooled CCD linear array *3* (1024 elements, sensitivity level 10 photon/reading in the spectral region from 350 to 900 nm). The signal brightness is pre-amplified (by up to $3 \cdot 10^4$) by an electro-optical converter (EOC) *2* (*2*, *3* is the CCD camera with brightness preamplifier). The spectral image from the EOC is transferred to the input of the linear CCD array by a wide-angle lens. Amplification in the EOC takes place at the instant the strobe pulse is applied (our experiment employed a strobe pulse of 1 μs duration). This provides for instrumental noise subtraction and allows the return signal spectra to be recorded at any level of solar illumination.

In the first diffraction order of the polychromator (grating of 300 lines/mm) the working range is 525 nm, and the spectral resolution is about 0.5 nm/channel, which is sufficient to record the fluorescence spectra of pollutants in water bodies. The polychromator design allows the first nine diffraction orders to be used and makes it possible to obtain a spectral resolution of up to 0.022 nm/channel. Thus we can record, for example, the fine structure of the emission spectra of a laser plasma.[4]

The linear CCD array and brightness amplifier are controlled by a specialized processor *12*, which is responsible for primary processing and accumulation of spectra. The spectra are then transferred to a personal computer. The processor *12* also controls the power supply of the Nd:YAG laser *1* (remaining components of the lidar are laser cooling system *11*, Nd:YAG emitter *8*, second-harmonic generator *9*, and third-harmonic generator *10*).

We conducted experiments of four types:

– a study of water, soil, and plant samples under laboratory conditions,

– *in situ* recording of the spectra of similar samples,

– recording of fluorescence spectra of different plants (mostly trees) at various distances from the laboratory window,

– mapping of pollution in the coastal zone of the Atlantic Ocean (near Rio de Janeiro) from on board a research vessel.

In all the experiments we used the second and third harmonics of the Nd:YAG laser as the sounding radiation exciting fluorescence and Raman spectra in the objects under study.

When calibrating the lidar, we obtained return-signal spectra of sea water sampled in the coastal zone of the Atlantic Ocean and distilled water with a resistivity of 14 MΩ/cm. The sea water was sampled in two regions of the Rio de Janeiro coastline. Fluorescence peaks were recorded from the dissolved organic matter (DOM) (maximum at 590 nm) and phytoplankton chlorophyll A (maximum at 685 nm), as well as the Raman peak (650 nm) of the stretching vibrations of water molecules. The concentration of each type of admixture can be determined by measuring the ratio of the fluorescence and Raman peaks.[1–3]

Figure 2 shows the fluorescence spectra of samples of Brazilian soil, vegetation, and sea water. The spectra were excited by the third harmonic of the Nd:YAG laser. For comparison, the spectra shown in the figure are scaled to the elastic scattering signal ($\lambda = 355$ nm). One can see that whereas the shapes of the return-signal spectra of the various samples are similar, the values of the fluorescence peaks of different pigments differ markedly. This fact makes it possible to compare different soils by their organic matter content and mineral composition. In particular, as can be seen from Fig. 2*a*, the fluorescence signals of phytoerythrite (near 630 nm) and chlorophyll (near 700 nm) for soil samples from the upper level of the water table markedly exceed those for the samples from the lower level. The difference in amplitudes of the return signals characterizes the organic matter content in the productive soil layer.

Figure 2*b* displays return-signal spectra of samples of soil (Mato Grosso do Sul), Atlantic Ocean water, and leaves of the *Pao Brazil* tree. As can be seen, the spectra from soil, sea water, and leaves have a similar structure, but the water spectrum contains additional Raman peaks of stretching O–H vibrations of water molecules ($\lambda = 407$ nm), and the leaf spectrum exhibits the more pronounced fluorescence spectrum of chlorophyll A and B ($\lambda = 690$ and 740 nm). The quantitative similarity of the spectral positions of all the principal fluorescence maxima of the mineral components and organic matter in the samples of soil, sea water, and plant material is likely a fundamental property of the Earth's surface and is indicative of a deep relation between the chemical composition of the upper soil layer, sea water, and vegetation.

Remote identification of plants is an important application of the lidar technique. An experiment was conducted on remote sensing of various tropical trees growing on mountainsides near the Catholic University of Rio de Janeiro (PCU Rio). The trees were sensed from the laboratory window. The distance to the objects varied from 40 to 550 m and was measured independently by a laser range finder. The Nd:YAG laser second harmonic radiation ($\lambda = 532$ nm) was directed by eye at the tree tops, and the return-signal spectra were recorded. The spectrum accumulation time did not exceed 5 s. Sample recorded spectra are shown in Fig. 3.

From Figs. 2–3 it can be seen that the fluorescence spectra of different types of trees differ markedly in shape for return signals recorded from distances up to 530 m. Thus, this technique enables remote identification and monitoring of the state of individual trees. This capability can be of use in assessing the state of forests and their specific composition.

Mapping of pollution of the Global Sea is urgent in connection with frequent discharges of pollutants into the environment. The lidar technique, which allows real-time *in situ* measurements of water

pollution, has indisputable advantages over all other traditional chemical methods, first, because the chemical composition of sea water varies rapidly, and already several hours (the characteristic time needed for delivery of the sample to a laboratory and for its chemical analysis) after sampling, the fluorescence spectrum of the sampled water can change significantly.

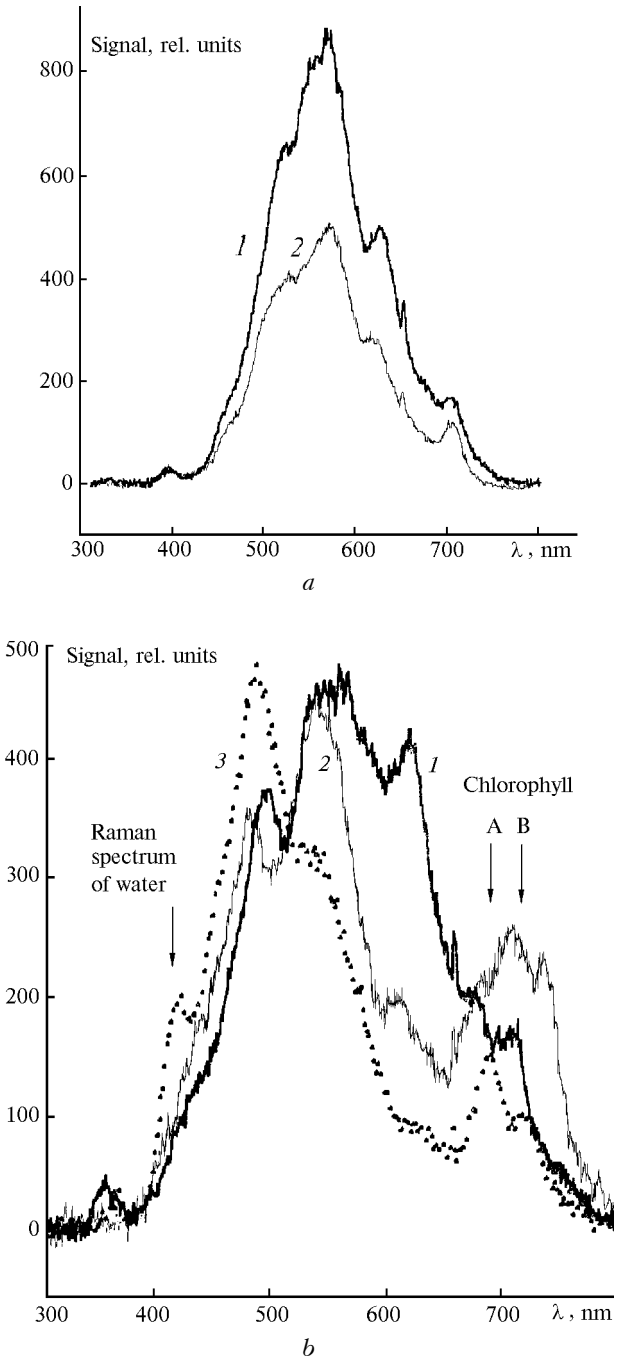

Fig. 2. Sample return-signal spectra of soil (the spectra were not compensated for the bandpass of the BS-7 cut-off light filter): the upper panel shows soil from Amazon, depth from 0 to 6 cm (curve *1*) and from 92 to 134 cm (curve *2*); the lower panel compares the return-signal spectra of soil (*1*), leaves (*2*), and sea water (*3*).

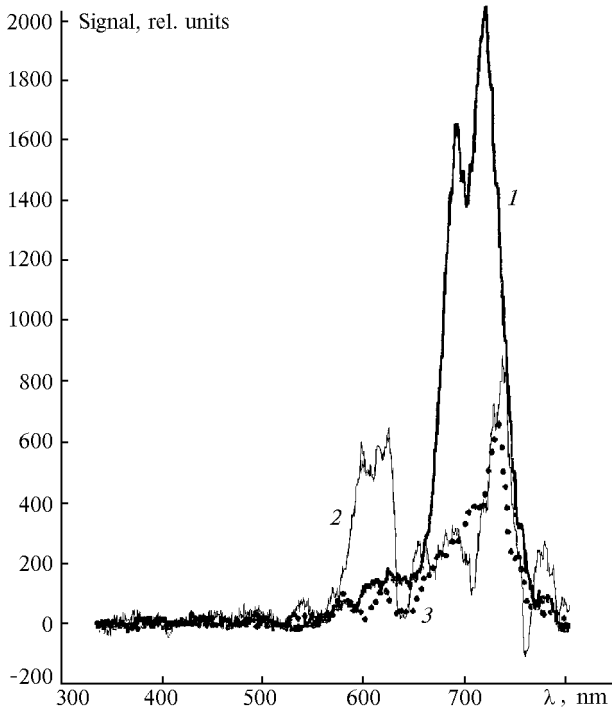

Fig. 3. Remote identification of plant type and state by fluorescence spectra excited by laser radiation at a distance of about 500 m: deciduous tree (curve *1*) and palms (curves *2* and *3*). Variations of spectral shape are noticeable from one sample to another.

Figure 4 shows a typical return-signal spectrum obtained in a field experiment conducted along the coast of the Atlantic Ocean in collaboration with the Rio de Janeiro municipal water monitoring service (FEEMA). The thick solid curve in Fig. 4 is for the Flamengo region, the dotted curve is for the Botafogo region, and the thin curve corresponds to the spectrum of distilled water. The arrows show the characteristic areas in the fluorescence spectra of organic matter and phytoplankton chlorophyll A, as well as the Raman signal of stretching vibrations of water molecules. Scaling of fluorescence signals to the Raman signal allowed us to compare the concentrations of fluorescent substances in different water samples. As can be seen, the distilled water sample contains organic matter in relatively high concentration.

The lidar system was mounted in a minibus, so we were able to conduct measurements immediately at the time of sampling and some time later. Water samples were collected in a quartz vessel, and the sounding laser beam was directed into the vessel from the top downward through the open surface by means of the metal mirror. The minibus moved along the shore with sampling stops every 2–3 km.

As can be seen from Fig. 4, the return-signal spectra vary widely from sample to sample in the fluorescence amplitude of both chlorophyll (peak at $\lambda = 685$ nm) and dissolved organic matter ($\lambda = 590$ nm). This reflects the variability of pollutant

content and chemical composition of the investigated water samples as a whole. Two hours after sampling, the return-signal spectra of the same samples were measured a second time. As it turned out, the shape of the spectrum changed markedly.

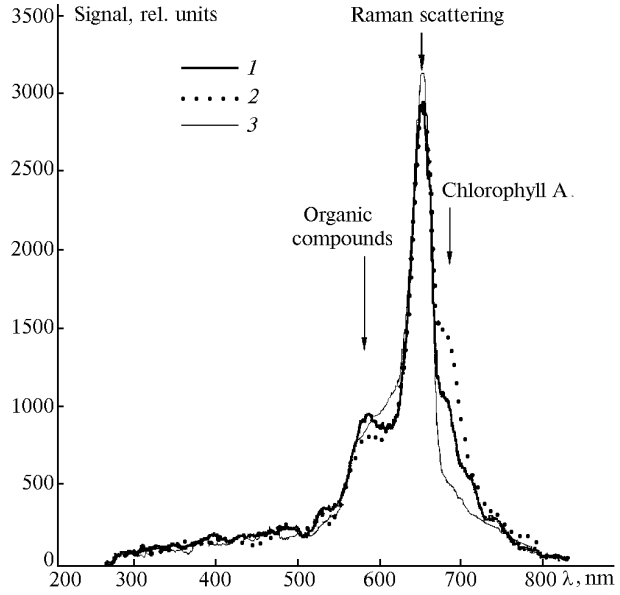

Fig. 4. Spectra of lidar return signals from water sampled in coastal areas of the Atlantic Ocean at different stations near Rio de Janeiro. The spectra were excited by second-harmonic radiation of a Nd:YAG laser (λ = 532 nm).

Figure 5 illustrates this fact. It shows the results of *in situ* measurements of the relative concentrations of organic matter and chlorophyll A in the samples of sea water from different regions of the coast near Rio de Janeiro (relative values of the fluorescence signal of chlorophyll are plotted along the abscissa, and relative values of the fluorescence signal of the dissolved organic matter are plotted as the ordinate). As can be seen, in all cases the fluorescence signal scaled to the Raman signal (λ = 655 nm) varied from sample to sample (the corresponding variations are shown by arrows). These changes are indicative of changes in the concentration of the corresponding pigments. Therefore, a true picture of pollution of a water body can be obtained only from airborne or shipborne lidar measurements.

In the course of this research, we conducted a field experiment in the vicinity of Port Makae, Rio de Janeiro, Brazil. The lidar system was installed in a container laboratory on the deck of a small ship (displacement about 500 t), the distance between the receiving telescope and the water surface not exceeding 50 m. The ship plied along the shore (maximum distance off shore was 20 miles) crossing an estuary, areas of underwater oil pipelines, as well as areas of heavy ship traffic. Some examples of the return-signal spectra recorded during this field experiment are shown in Fig. 6.

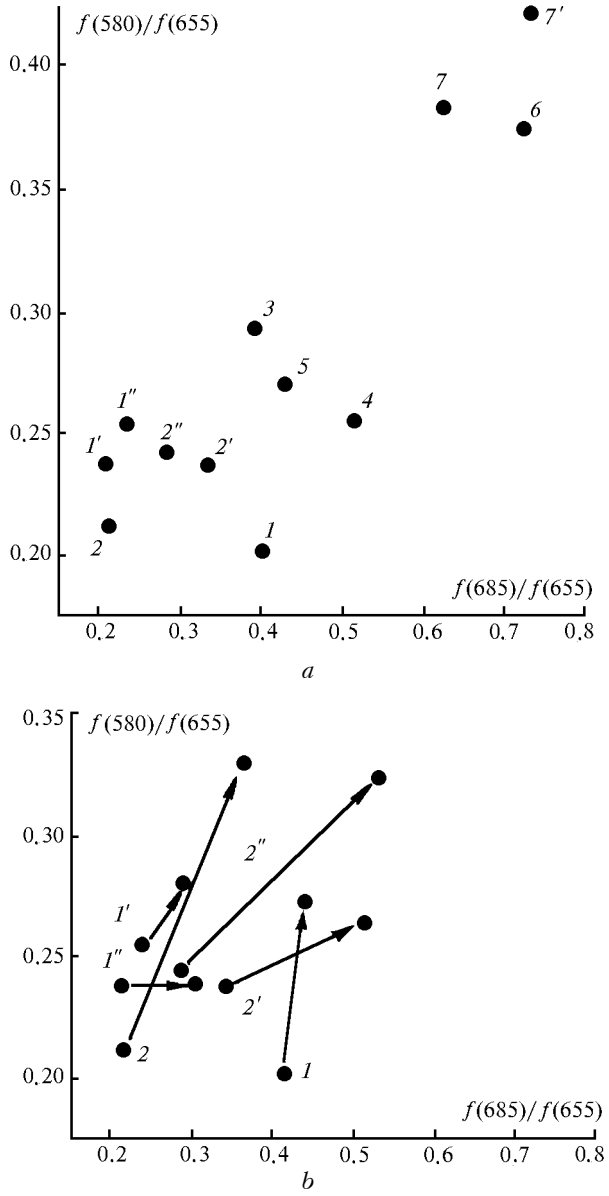

Fig. 5. Relative concentrations of chlorophyll A (abscissa) and dissolved organic matter (ordinate) in Atlantic Ocean water sampled on January 27, 1997, at different stations near Rio de Janeiro: Pepe (*1*), Pepino (*1′*), H. Nacional (*1″*), Leblon (*2*), V. de Albuquerque (*2′*), B. Mitre (*2″*), Copacabana (*4*), Botafogo (*6*), Flamengo (*7*), Gloria (*7′*); results obtained immediately after sampling (*a*) and these same results together with results obtained 2 h after sampling (shown by arrows) (*b*).

Figure 6*a* shows spectra of return signals recorded as the ship moved off shore. The peaks from left to right correspond to fluorescence signals of dissolved organic matter, Raman spectrum of water, and fluorescence signals of chlorophyll. As can be seen, the concentrations of dissolved organic matter and chlorophyll decrease with time (with distance from shore). Fluorescence signals of chlorophyll A (λ = 685 nm) and dissolved organic matter (λ = 580 nm) fall off rapidly, while the Raman signal

of water (λ = 650 nm) remains unchanged. Figure 6*b* presents examples of return-signal spectra (for excitation by the third harmonic of the Nd:YAG laser at λ = 355 nm). The spectra were obtained in a region of possible anthropogenic pollution, since at just this spot a river running past industrial installations empties into the ocean. Here also are located oil terminals and underwater pipelines. The ship moved in a region of mixed river and ocean water at a speed of 7 knots. It can be seen that the shape of the spectrum varies rapidly, and the spectrum contains components corresponding to mineral and organic material, as well as fluorescence peaks of phytoplankton (in the region from 600 to 800 nm). The concentration and composition of dissolved organic matter as well as the chlorophyll A content in the region under study exhibited characteristic large variations (spectra were recorded with the interval of 3 min). This is indicative of the possible presence of anthropogenic pollution sources in the investigated region during our measurements.

Global monitoring of the temperature of the upper ocean layer is one of the routine tasks of oceanography. Such measurements are urgent both because of the needs of weather forecasting and in view of the problem of global warming. The water temperature is currently measured mainly by contact methods using buoys which then transmit information to satellites or onshore stations. Because of the limited number of buoys and their relatively short service life, these measurements are of a fragmentary character and cannot cover the entire surface of the Global Ocean. Among remote sensing methods suitable for airborne (or spaceborne) use, the method based on radiometric measurement of the brightness temperature of the water surface may be mentioned (see, for example, Ref. 5). However, this method can measure only the temperature in a thin water layer (thickness within several tens of microns). This temperature depends heavily on climatic conditions at the time of measurement (cloudiness, sea state, evaporation rate, precipitation), and therefore differs significantly from the actual, "physicalB temperature of the upper ocean layer.

Hoge, Wright, and Swift[6] proposed another method for measuring the temperature of the Global Ocean which could be an alternative to the one mentioned above. This method is based on the temperature dependence of the Raman band of stretching O–H vibrations of water molecules. According to Ref. 6, the "physicalB temperature of a water body can be measured to within 1–2°C. To do this, it is necessary to resolve the Raman band into its individual lines, then during the field experiments determine the changes in the spectroscopic parameters of these lines, and compare them with the data of laboratory measurements. However, it has turned out in practice that resolving the Raman band into its components is an ambiguous procedure, especially in the case of field measurements, because the band profile in this case is distorted by solar illumination and the fluorescence signal of organic matter contained in the sea water in the Stokes spectral region. That is why this method has not found wide practical application in oceanography.

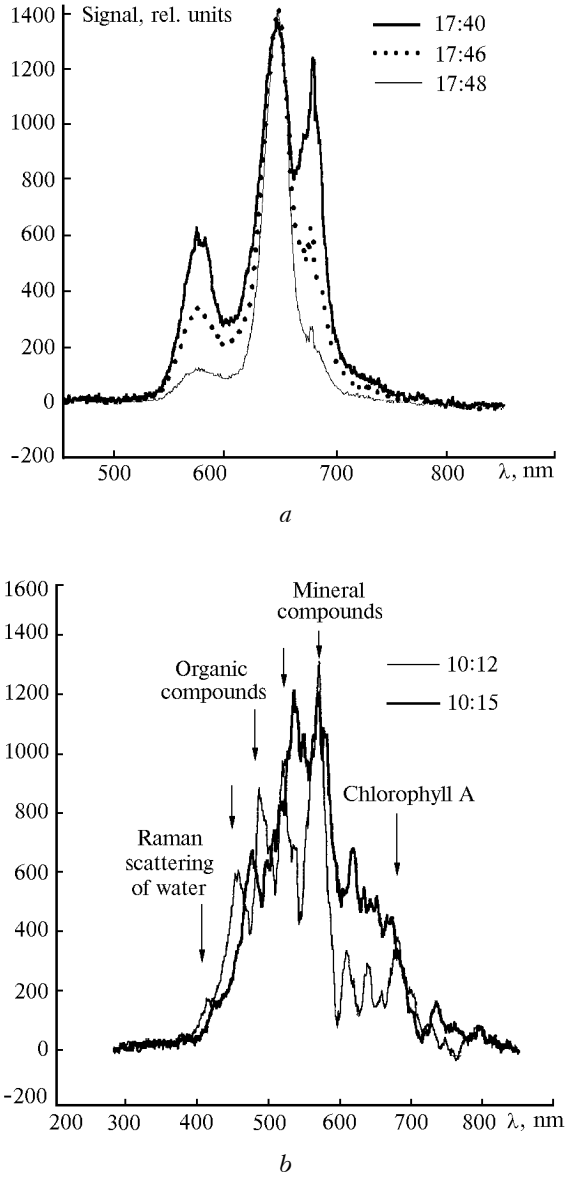

Fig. 6. Spectra of return signals from sea water recorded on board a research vessel in the Atlantic Ocean (near Makae) on May 12 and 13, 1997 (local time is shown near the curves): spectra obtained using the second (*a*) and third (*b*) harmonics of the Nd:YAG laser.

In our recent paper[7] we proposed a new method for remote measurement of water (including sea water) temperature, based on a special procedure for processing the Raman band profile and tested under laboratory conditions. The proposed method does not require that the Raman profile be resolved into its components.

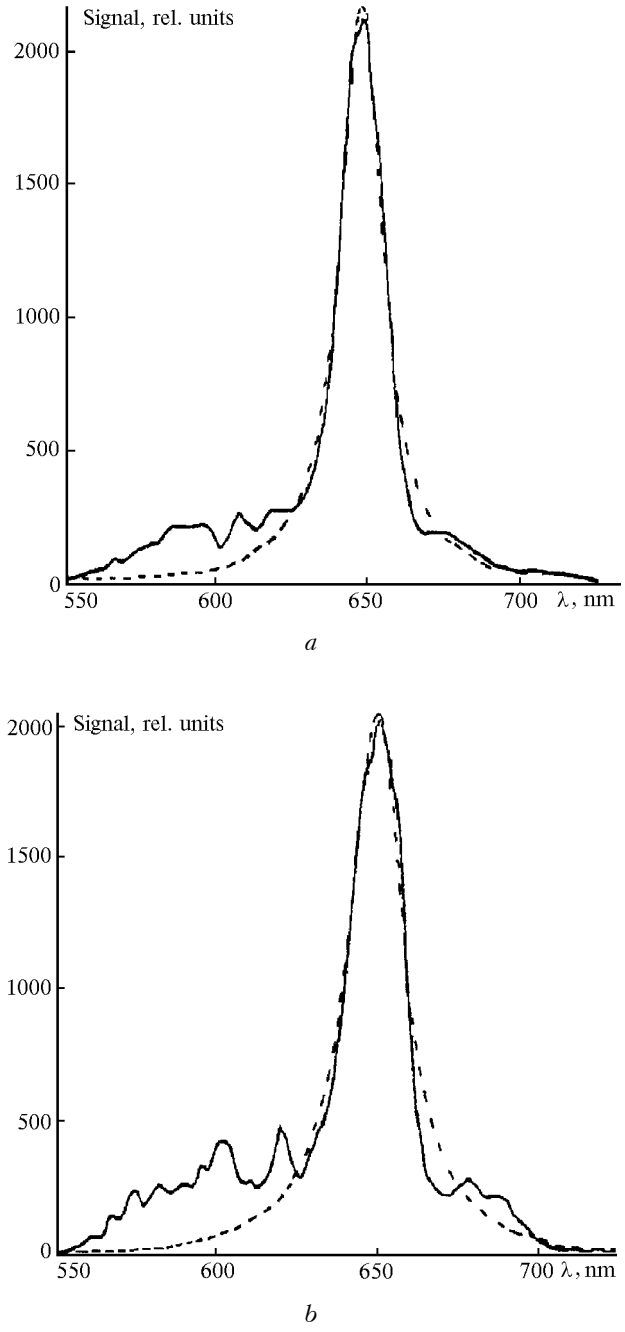

Fig. 7. Sample shipborne lidar Raman spectra of ocean water recorded using the Nd:YAG second harmonic (fourth diffraction order of the polychromator). The dashed lines plot the approximating Lorentz profiles: spectra measured at 11:09 (*a*) and 11:08 L. T. (*b*); the centers of the Lorentz profiles are at 648.36 and 648.48 nm; the water temperature was 24.6 and 24.9 °C (as measured by a temperature sensor).

During the experiment we tested the possibility of making remote measurements of ocean temperature under field conditions. Figure 7 shows spectra of the Raman stretching band of the sampled sea water. The spectra were recorded at an interval of 1 min from a distance of 50 m [slight sea (sea state around 2 balls), at a speed of 8 knots], the calculated effective sounding depth was 50 cm, the measurements were made in the fourth diffraction order of the polychromator. Singularities in the wings (see Fig. 7) are caused by contributions of fluorescence of dissolved organic matter and phytoplankton chlorophyll A; the dashed line plots an approximation of the Raman band by a Lorentz profile.

In parallel, the temperature of the upper ocean layer was measured by an electronic thermometer with a calibrated thermoresistor. The measurements show that the ocean temperature varied from 21 to 25 °C (these fluctuations can be explained by variations in the submerged depth of the thermometer due to the action of waves produced by the motion of the ship). According to the results of our laboratory experiments,[7] as the water temperature increases, the center of the approximating profile shifts toward the Stokes region at the rate of 1 cm^{-1}/deg. The difference in the spectral positions of these profiles observed in the field experiment did not exceed 5 cm^{-1} (in particular, in Fig. 7 it is 2.7 cm^{-1}), i.e., it agrees with the temperature difference measured by the thermoresistor. More accurate contact measurements of the vertical profile of the ocean temperature will likely allow us to draw a final conclusion on the applicability of the proposed methods to remote measurements of water temperature.

Conclusion

To sum up, we have shown that the developed lidar is capable of successfully solving a wide variety of problems arising in the ecological monitoring of the Global Ocean. The lidar can be installed onboard aircraft, helicopters, motor vehicles, and ships.

Parallel measurements of the fluorescence spectra of soil, plants, and sea water have revealed the common spectral features of these objects. Remote laser identification of the types of trees and determination of the presence of stresses in vegetation can be used in the global monitoring of forests, as well as for routine monitoring of national parks. The temporal variability of the return-signal spectra of sea water samples is indicative of the need for fast *in situ* analysis of water media. This underscores the advantages of remote laser measurements of the state of environmental objects, especially in hard-to-reach areas.

The use of the described lidar opens up the possibility (with the use of a satellite navigation system) of plotting “instantaneousB (on the scale of characteristic evolution times of the upper ocean layer) maps of the pollution of large water bodies in the zones of industrial accidents, near big cities, ship routes, and other areas where real-time information on the ecological state of the water medium is needed.

Acknowledgments

The authors are grateful to Professor R.A. Nunes and Professor L.S. Skavarda de Karmo (PCU, Rio), as well as I. Karavalio and R. Tabares for their help in this work.

This work was partially supported by the CNPq, FEEMA, EMBRAPA, and PetroBraz (Brazil), and by the Russian State Programs "Fundamental MetrologyB and "Fundamental SpectroscopyB as well as the Russian Foundation for Basic Research, Grants No. 99–02–16591 and No. 98–02–16074.

References

1. R.M. Measures, *Laser Remote Sensing. Fundamentals and Applications* (John Wiley & Sons, New York–Toronto–Singapore, 1985), 542 pp.
2. A.F. Bunkin, D.V. Vlasov, and D.M. Mirkamilov, *Physical Principles of Airborne Laser Sounding of the Earth's Surface* (FAN, Tashkent, 1987), 271 pp.
3. F.E. Hoge and R.N. Swift, Appl. Opt. **20**, No. 18, 3197–3205 (1981).
4. A.F. Bunkin, M.A. Davydov, A.V. Rezov, A.L. Surovegin, and D.Yu. Tsipenyuk, Laser Physics **4**, No. 6, 1198–1201 (1994).
5. R.C. Smith, O.B. Brown, F.E. Hoge, et al., Appl. Opt. **26**, No. 11, 2068–2081 (1987).
6. F.E. Hoge, C.W. Wright, and R.N. Swift, Appl. Opt. **26**, No. 11, 2082–2094 (1987).
7. A. Chedin, N.A. Scott, and A. Berroin, J. Appl. Meteorol. **21**, No. 4, 613–618 (1982).
8. D.A. Leonard, B. Caputo, and F.E. Hoge, Appl. Opt. **18,** 1732 (1979).
9. A.F. Bunkin and S.M. Pershin, BRAS. Physics of Vibrations **61**, No. 3, 158–163 (1997).